Native and Methylated Cyclodextrins with Positive and Negative Solubility Coefficients in Water Studied by SAXS and SANS

ARTICLE *in* THE JOURNAL OF PHYSICAL CHEMISTRY B · OCTOBER 2008

Impact Factor: 3.3 · DOI: 10.1021/jp802031w · Source: PubMed

4 AUTHORS:

André Kusmin
Delft University of Technology
10 PUBLICATIONS **69** CITATIONS
SEE PROFILE

Ruep Ekkehard Lechner
European Spallation Source
169 PUBLICATIONS **2,491** CITATIONS
SEE PROFILE

Martin Kammel
Physikalisch-Technische Bundesanstalt
32 PUBLICATIONS **246** CITATIONS
SEE PROFILE

Wolfram Saenger
Freie Universität Berlin
625 PUBLICATIONS **32,876** CITATIONS
SEE PROFILE

Native and Methylated Cyclodextrins with Positive and Negative Solubility Coefficients in Water Studied by SAXS and SANS

André Kusmin,[†,‡,#] Ruep E. Lechner,[§,‡] Martin Kammel,[§] and Wolfram Saenger*[,†,‡]

Institute for Chemistry and Biochemistry/Crystallography, Freie Universität Berlin, Taku Str. 6, 14195 Berlin, Germany, International Graduate College, Freie Universität Berlin, Taku Str. 3, 14195 Berlin, Germany, Hahn-Meitner-Institut Berlin, Glienicker Str. 100, 14109 Berlin, Germany, and Institut für Festkörperforschung, Forschungszentrum Jülich, 52425 Jülich, Germany

Received: March 7, 2008; Revised Manuscript Received: July 17, 2008

While the solubility of native α-, *β*-, *γ*-cyclodextrins (CDs) in water rises with temperature, the opposite is true for their methylated derivatives (mCDs; per-dimethylated *β*-CD and per-trimethylated *γ*-CD). The mCDs are well-soluble in cold water and crystallize upon heating, which we associate with the hydrophobic effect. To study the hydrophobic effect and hydration of CDs and mCDs dissolved in water (D_2O), we performed small-angle X-ray and neutron scattering (SAXS and SANS) measurements. The experimental scattering curves were put on absolute scale and compared to scattering curves calculated from crystal structures using the cube method. The results of the comparison indicate that (i) in solution, CDs and mCDs are in monomeric form, (ii) van der Waals and solute excluded volumes can be related by introducing a shell of a thickness that correlates with the solute's structure and solute−water interactions, and (iii) the SAXS curves calculated under the assumption of a uniform distribution of electron density in the solute molecules agree with experimental ones for CDs, but not for mCDs. The temperature and concentration dependence of SAXS curves is significant for mCDs and weak for CDs and is discussed in terms of solute−solute interactions. Specifically, these interactions become more attractive in solutions of mCDs with increasing temperature, concentration, or both, in accord with mCDs' negative temperature coefficient of solubility in water.

1. Introduction

The α-, *β*-, and *γ*-cyclodextrins (CDs) are a family of doughnut-shaped cycloamyloses composed of six, seven, and eight D-glucoses linked by α(1−4) bonds.[1] CDs and their derivatives are primarily known for their ability to form inclusion complexes in aqueous solutions and in the crystalline state with molecules that are able to fit completely or partially into their central cavity[1] (Figure 1a). It is less known that the CDs per-dimethylated at all of their O2 and O6 or per-trimethylated at all of their O2, O3, and O6 hydroxyl groups (Figures 1b, 2) are better soluble in cold water than in hot water, where they finally form crystalline precipitates.[2] That is, the solubility coefficient in water is negative for methylated CDs (mCDs), but it is positive for native CDs, as their solubility rises with increasing temperature.[3]

Aqueous solutions of per-dimethylated heptakis(2,6-di-O-methyl)-*β*-cyclodextrin (DIMEB) and of per-trimethylated octakis(2,3,6-tri-O-methyl)-*γ*-cyclodextrin (TRIMEG) crystallize as anhydrate[4] and dihydrate,[5] respectively, from hot water (50 to 70 °C), but as highly hydrated DIMEB·$15H_2O$[6] and TRIMEG·$4.5H_2O$[7] from cold water (18 °C). In DIMEB·$15H_2O$, the water molecules form a channel-type clathrate hydrate that encloses DIMEB as guest molecules. This prompted us to suggest[6,7] that mCDs feature well-ordered hydration shells at low temperatures and are therefore very soluble. At higher temperatures, however, water molecules would become more mobile, thereby abolishing the ordered hydration, and the hydrophobic mCD molecules start to aggregate and crystallize. This view was supported in a theoretical study[8] which indicated that *β*-CD is equally well-hydrated at 25 and 70 °C whereas for DIMEB, hydration is much better at 25 °C than at 70 °C. To test this hypothesis experimentally, we performed quasielastic neutron scattering (QENS) studies, but for their full analysis with regard to hydration shell, quantitative data on solute−solute interactions were lacking.[9] To get such data, we measured (to our knowledge, for the first time) small-angle X-ray and neutron scattering (SAXS and SANS) on D_2O solutions of *β*- and *γ*-CD, DIMEB, and TRIMEG.

Aqueous solutions of CDs and mCDs are good model systems to study hydrophobic interactions and hydration, because in contrast to protein or nucleic acid solutions, electrostatic interactions can be neglected, since CDs and mCDs bear no charges. In addition, since CDs and mCDs are small and their structures are well-characterized, the analysis of their small-angle scattering spectra may go beyond the common procedures applied in studies of bigger and more complex molecules.

In this work, we characterize the form in which the studied compounds are present in solution and compare the scattering by dilute solutions to the scattering curves calculated from crystal structures. We show that the solute excluded volume can be presented as a sum of solute's van der Waals volume and a shell with a thickness that correlates with solute's structure and solvent−solute interactions. Finally, we discuss the temperature and concentration dependence of solute−solute interactions, compare it to the literature data on osmotic pressure

* Corresponding author. Institute for Chemistry and Biochemistry/Crystallography, Phone: +49(30)-838-53412. Fax: +49(30)-838-56702. E-mail: saenger@chemie.fu-berlin.de.
† Institute for Chemistry and Biochemistry/Crystallography, Freie Universität Berlin.
‡ International Graduate College, Freie Universität Berlin.
§ Hahn-Meitner-Institut Berlin.
# Institut für Festkörperforschung, Forschungszentrum Jülich.

10.1021/jp802031w CCC: $40.75
Published on Web 09/18/2008

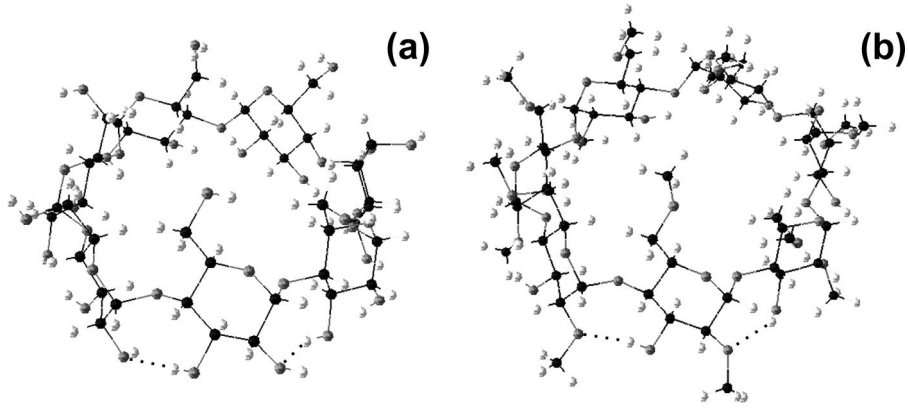

Figure 1. X-ray crystal structures for β-CD[22] (a) and DIMEB[24] (b). Carbon, oxygen, and hydrogen atoms are black, gray, and light gray, respectively. Note that O3−H···O2 hydrogen bonds (shown by dotted lines for only 3 glucoses, but they are formed all around the CD and mCD macrocycles) stabilize the "round" structure of DIMEB. They are not possible in TRIMEG because O3−H is also methylated, giving rise to more structural flexibility of the macrocycle.

TABLE 1: Physical Parameters Derived for Native and Methylated CDs[a]

	M	*EX*	V_{THEO}	ρ_{AV}	$\Delta\rho_{AV}$	$R^2_{g(EXP)}$[b]	$R^2_{g(THEO)}$	D_{EXP}[b]	D_{THEO}
SAXS; electron scattering density of D_2O: $\rho_0 = 0.0934$									
β-CD	1134	0.23	1200	0.1416	0.0482	42.3(0.4)[c]	41.1	19.0	18
γ-CD	1297	0.10	1302	0.1489	0.0555	53.2(0.2)[c]	49.7	19.0	19.7
DIMEB	1331	0.26	1575	0.1277	0.0343	31.5(0.5)[c]	45.2	18.8	20.3
TRIMEG	1633	0.33	2125	0.1167	0.0233	22.1(0.4)[c]	56.0	10.2	23.1
SANS; neutron coherent scattering length density of D_2O: $\rho_0 = 0.06344$									
DIMEB	1331	0.26	1575	0.01789	−0.04555	61.7(0.9)[c]	45.2	28	20.3

[a] Molecular mass (*M*), parameter *EX*, excluded volume (V_{THEO}), average scattering density (ρ_{AV}), scattering contrast ($\Delta\rho_{AV}$), experimental and computed (in homogeneous approximation) squares of gyration radius ($R^2_{g(EXP)}$ and $R^2_{g(THEO)}$, respectively), and experimental and computed maximum diameters of the solute molecule (D_{EXP} and D_{THEO}, respectively). ρ_0, ρ_{AV} and $\Delta\rho_{AV}$ are given in 10^{-12} cm/Å^3, R^2_g in Å^2, *EX* and D in Å and V_{THEO} in Å^3; $\Delta\rho_{AV} = \rho_{AV} - \rho_0$. (For X-ray, ρ = number of electrons per Å^3 multiplied by the scattering length of an electron, r_0, $r_0 = 0.282 \times 10^{-12}$ cm, see e.g. ref 13. For SANS, ρ is the sum of neutron coherent scattering lengths divided by the excluded volume.) [b] $R^2_{g(EXP)}$ and D_{EXP} were determined: for SAXS, from the curves shown in Figure 3; for SANS, from the curve for $c = 6.6$ mg/mL shown in Figure 8a. [c] Standard deviations obtained from the linear fit.

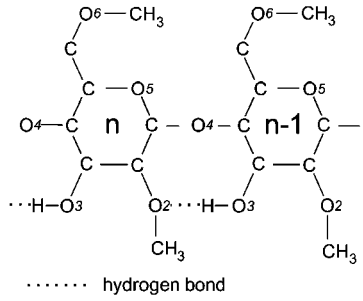

Figure 2. Two adjacent and hydrogen bonded glucose units of DIMEB.

measurements, and interpret the results in terms of the sticky hard sphere[10] model.

2. Experimental Section

D_2O 99.9% pure and β-CD (Aldrich), TRIMEG > 97%, and DIMEB > 98% (CycloLab), γ-CD > 98% (ROTH) were used without further purification. All solutions were filtered (Millipore, 0.22 μm) after preparation, their densities were calculated from the density of pure D_2O and from the excluded volumes (V_{THEO}) that were computed by the cube method for $EX = 0$ (see section 3.1).

Synchrotron radiation X-ray scattering data were collected on the X33 camera of EMBL at the storage ring DORIS III (DESY, Hamburg, Germany).[11] Solutions in D_2O of β-CD (6.0 mg/mL {5.3 mM}), γ-CD (9.3, 20.9, 42.9 mg/mL {7.1, 16.1, 33.1 mM}), DIMEB (6.6, 14.9, 25.9, 44.3, 50.0, 76.0 mg/mL {4.9, 11.2, 19.4, 33.3, 37.5, 57.1 mM}), and TRIMEG (10.0, 16.9, 35.1, 64.1, 90.2 mg/mL {6.1, 10.3, 21.5, 39.3, 55.2 mM}) were measured in the temperature range 20−70 °C. The measurement time of a single SAXS pattern was 3 min. The data were recorded using a MAR345 image plate detector at a sample−detector distance of 2.7 m and a wavelength of $\lambda = 1.5$ Å, covering the range of momentum transfer $0.012 < Q < 0.50$ Å^{-1} ($Q = 4\pi \sin\theta/\lambda$, where 2θ is the scattering angle). The data were averaged after normalization to the intensity of the incident beam using the program package PRIMUS.[12]

The experimental SAXS curves (intensities versus Q), $I_{EXP/SAXS}(Q,c)$, were found from the D_2O and sample SAXS patterns ($I_{D2O/SAXS}(Q)$ and $I_{S/SAXS}(Q,c)$, respectively) as follows:

$$I_{EXP/SAXS}(Q,c) = \{I_{S/SAXS}(Q,c) - I_{D2O/SAXS}(Q)\} \times f_{H2O}/(c \times N_a/M) \quad (1)$$

where c is the solute concentration [g/mL], N_a is Avogadro's number, and M is the molecular mass of the solute molecule [g/mol], see Table 1. The factor f_{H2O} normalizes[13] the data measured in D_2O solution to the scattering by H_2O, and is defined as

$$f_{H2O} = I_{H2O}(0)/(I_{H2O} - I_{E.C.}) \quad (2)$$

where $I_{H2O}(0)$, the zero-angle X-ray scattering of H_2O, is 0.01632 cm^{-1} at 20 °C.[13] The denominator of eq 2 is the

difference in the measured scattering intensity between the H_2O filled (I_{H2O}) and empty cell ($I_{E.C.}$) and provides the scattering by H_2O. Since I_{H2O} was measured for our cell and the ratio $I_{H2O}/I_{E.C.}$ was known to be $\approx 1.34 \pm 0.05$, we could evaluate f_{H2O} that was necessary to put the sample SAXS curves on an absolute scale. In the following, $I_{EXP/SAXS}(Q,c)$ is given in barn [1 barn $= 10^{-24}$ cm^2]. Because in the low Q region the sample scattering was weak compared with the scattering by the cell, the SAXS curves were analyzed only for $Q > 0.05$ Å^{-1}.

The SANS spectra of DIMEB solutions in D_2O in the temperature range 20−60 °C (for one concentration only, 44.0 mg/mL{33.1 mM}) and at 25 °C for 6.6, 32.2, 44.3 mg/mL {4.9, 24.2, 33.3 mM} were recorded at the small-angle scattering spectrometer V4[14] (BENSC, Hahn-Meitner Institute, Berlin). The data were collected at two sample−detector distances (1 and 4 m) with a wavelength of 6.07 Å, covering the range of momentum transfer $0.02 < Q < 0.37$ Å^{-1}. The measurement time of a single SANS pattern was 5 min. The data were reduced and normalized to H_2O scattering[15] with the program BerSANS,[16] rendering SANS patterns $I_{S/SANS}(Q,c)$. The experimental SANS curves, $I_{EXP/SANS}(Q,c)$ [barn], were obtained for different concentrations (c) and corrected for background (I_{INC}, incoherent scattering by DIMEB and by D_2O {583 and 0.325 barn per molecule, respectively}):

$$I_{EXP/SANS}(Q, c) = \{I_{S/SANS}(Q, c)/(c \times N_a/M)\} - I_{INC} \quad (3)$$

3. Data Analysis

The method of small-angle X-ray and neutron scattering and its applications have been the subject of many publications, and equations not explicitly referenced here can be found elsewhere; for example, see refs 17 and 18.

3.1. Single Molecule Scattering. The scattering from an infinitely dilute solution, $I_{THEO}(Q)$, is[19,20]

$$I_{THEO}(Q) = \langle |F(\boldsymbol{Q}) - f(\boldsymbol{Q})|^2 \rangle_\Omega \quad (4)$$

where $\langle ... \rangle_\Omega$ stands for averaging over all orientations of vector $\boldsymbol{Q}$ with respect to the solute molecule. The scattering amplitude of the molecule in vacuum, $F(\boldsymbol{Q})$:

$$F(\boldsymbol{Q}) = \sum_{i=1}^{N} b_i \exp(-i\boldsymbol{Q} \cdot \boldsymbol{r}_i) \quad \text{(SANS)} \quad (5)$$

$$F(\boldsymbol{Q}) = \int_V \rho(\boldsymbol{r}) \exp(-i\boldsymbol{Q} \cdot \boldsymbol{r}) d\boldsymbol{r} \quad \text{(SAXS)} \quad (6)$$

where b_i [cm] is the neutron coherent scattering length of the ith atom, $\boldsymbol{r}_i$ is the vector (in the molecule's center of mass coordinate system) pointing to the ith atom, N is the number of all atoms (including hydrogens) in the molecule, and $\rho(\boldsymbol{r})$ is the electron density. The scattering amplitude of the volume excluded by the molecule in solution (V, excluded volume hereafter) when this volume is filled by solvent, $f(\boldsymbol{Q})$, is

$$f(\boldsymbol{Q}) = \rho_0 \int_V \exp(-i\boldsymbol{Q} \cdot \boldsymbol{r}) d\boldsymbol{r} \quad (7)$$

where ρ_0 is the neutron coherent scattering length density of the solvent in SANS and solvent's electron density in SAXS. Equation 4 may be written as

$$I_{THEO}(Q) = \langle | \int_V \Delta\rho(\boldsymbol{r}) \exp(-i\boldsymbol{Q} \cdot \boldsymbol{r}) d\boldsymbol{r}|^2 \rangle_\Omega$$

$$= 4\pi \int_0^\infty \gamma(r) \frac{\sin Qr}{Qr} r^2 dr \quad (8)$$

where $\Delta\rho(\boldsymbol{r}) = \rho(\boldsymbol{r}) - \rho_0$. The average values of $\Delta\rho(\boldsymbol{r})$ and $\rho(\boldsymbol{r})$ over the excluded volume are $\Delta\rho_{AV}$ and ρ_{AV}, respectively. The correlation function $\gamma(r)$ is

$$\gamma(r) = \langle \int_V \Delta\rho(\boldsymbol{u}) \Delta\rho(\boldsymbol{u} + \boldsymbol{r}) d\boldsymbol{u} \rangle_\Omega \quad (9)$$

and can be evaluated without the knowledge of the three-dimensional electron density map (i.e., $\rho(\boldsymbol{r})$) assuming the electron density of the molecule to be uniform (homogeneous approximation). In this case, $\Delta\rho(\boldsymbol{u}) = \Delta\rho_{AV}$ if the vector $\boldsymbol{u}$ points to anywhere within the excluded volume, and $\Delta\rho(\boldsymbol{u}) = 0$ otherwise.

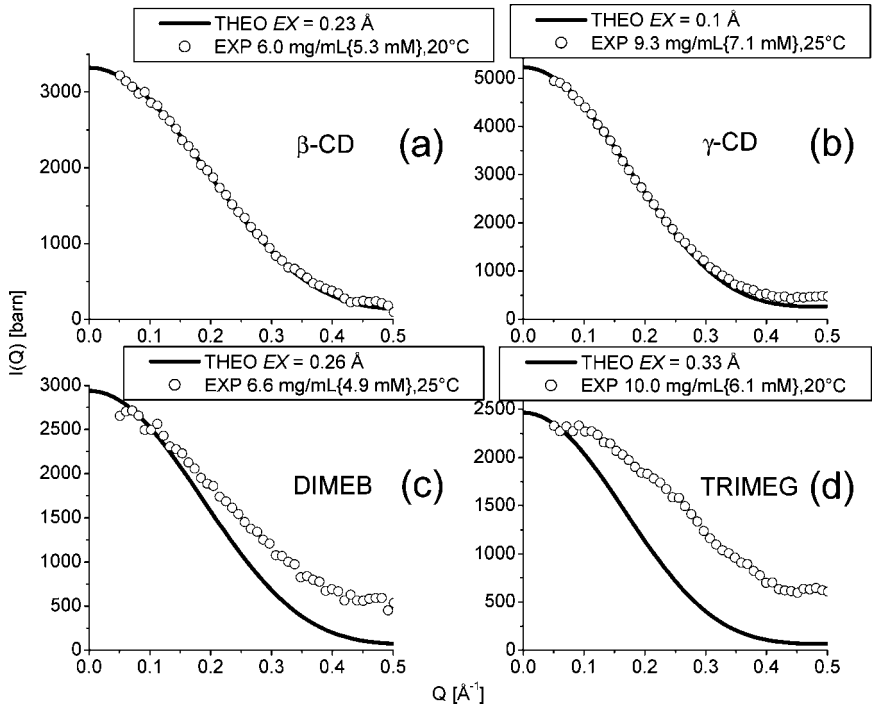

Figure 3. Experimental (EXP) and theoretical (THEO) SAXS for CDs and mCDs dissolved in D_2O.

The cube method[19,20] was applied to calculate (i) the theoretical SANS curve, $I_{THEO/SANS}(Q)$, from eqs 4, 5, 7 and (ii) under homogeneous approximation, the correlation function $\gamma_{THEO}(r)$ and the theoretical SAXS curve, $I_{THEO/SAXS}(Q)$, from eqs 8 and 9. In short, a molecule with a known crystal structure is put into a box which is then subdivided into small cubes (with edges of 0.4 Å used in this work). We define atom's maximal radius of exclusion as the sum of atom's van der Waals (vdW) radius and a (generally atom-dependent) parameter *EX*. All cubes that are within the maximal radius of exclusion of one particular atom belong to the volume excluded by this atom. The distances from all atoms (including hydrogens) of the solute molecule to one particular cube are evaluated and then compared to the corresponding maximal radii of exclusion of these atoms. If the cube is within the maximal radius of exclusion for at least one atom, it is attributed to the solute molecule's excluded volume. If not, it is attributed to the solvent. This attribution procedure eventually assigns to the solvent those cubes that actually belong to small voids within the molecule's vdW volume (and which are not accessible to solvent). This is corrected by a procedure used in a program written by us where, for every cube previously attributed to the solvent, it is tested whether this cube can belong to a continuous solvent-filled space big enough to accommodate a solvent molecule. If it is not, then the cube is reattributed to the excluded volume. Finally, the integration in eqs 7 and 9 turns into a summation over all cubes belonging to the excluded volume.

The excluded volume obtained by the cube method (V_{THEO}), its shape, and the calculated scattering curves ($I_{THEO}(Q)$) depend on the *EX* values of atoms on the surface of the molecule. An effective, atom-independent *EX* value can be obtained from the SAXS or SANS experiment. To show that, we write eq 8 as[21]

$$I_{THEO}(Q) = (\Delta\rho_{AV})^2 I_0(Q) + \Delta\rho_{AV} I_{01}(Q) + I_1(Q) \quad (10)$$

where $(\Delta\rho_{AV})^2 I_0(Q)$ is the scattering calculated under homogeneous approximation. The terms $I_{01}(Q)$ and $I_1(Q)$ arise due to a nonuniform distribution of scattering length and are negligible at low Q values.[21] Consequently, the effective *EX* value (in the following simply *EX*) can be found from the condition that $I_{THEO}(Q)$ coincides with $I_{EXP}(Q)$ in the low Q region. Because cyclodextrins are small molecules, the incoherent background in SANS is not negligible even at low Q's; therefore, we used SAXS spectra for determination of *EX* values. For SAXS, eq 10 may be written as

$$I(Q \rightarrow 0) = ((\rho_{AV} - \rho_0)V)^2 = N_e^{\,2} - 2N_e\rho_0 V + (\rho_0 V)^2 \quad (11)$$

where N_e is the number of electrons in the molecule. Clearly, the effective *EX* value guarantees that V_{THEO} is equal to the excluded volume (V) observed in the scattering experiment.

The computations were done using the crystal structures of CDs and mCDs studied here,[7,22−24] with vdW radii taken[25] as 1.75, 1.58, and 1.1 Å for C, O, and H atoms, respectively. All $I_{THEO/SAXS}(Q)$ and $I_{THEO/SANS}(Q)$ curves are in barn. The obtained *EX* values are in Table 1.

The part of the experimental scattering curves for $0.1 < Q < 0.2$ Å^{-1} was used to evaluate the intensity at $Q = 0$, $I_{EXP}(0)$, and the square of the radius of gyration, $R^2_{g(EXP)}$, using Guinier's law:

$$I_{EXP}(Q) = I_{EXP}(0) \times \exp(-R^2_{g(EXP)}Q^2/3) \quad (12)$$

The R^2_g value in the homogeneous approximation, $R^2_{g(THEO)}$, was obtained from $\gamma_{THEO}(r)$ (see eq 9 in ref 17). In general,[21]

$$R^2_g(\Delta\rho_{AV}) = R^2_{g(THEO)} + \alpha/\Delta\rho_{AV} - \beta/(\Delta\rho_{AV})^2 \quad (13)$$

If $\rho_S(\boldsymbol{r})$ is the deviation of the scattering density from the average value, $\rho_S(\boldsymbol{r}) = \rho(\boldsymbol{r}) - \rho_{AV}$, then[21]

$$\alpha = V^{-1}\int_V \rho_S(\boldsymbol{r})\boldsymbol{r}^2 d\boldsymbol{r} \quad (14)$$

$$\beta = V^{-2}\int_V\int_V \rho_S(\boldsymbol{r})\rho_S(\boldsymbol{r}')\boldsymbol{r}\cdot\boldsymbol{r}'\, d\boldsymbol{r}d\boldsymbol{r}' \quad (15)$$

To estimate the maximum diameter of the molecule, D_{EXP}, we calculated the spatial cosine transform of $I_{EXP}(Q,c)$, F(r)

$$F(r) = \int_0^\infty I_{EXP}(Q,c)\cos(Qr)dQ \quad (16)$$

and used the condition[26] that F(r) is zero for $r > D_{EXP}$. Because the so-obtained function F(r) oscillated around zero at high r values, we took as D_{EXP} the first r value for which $F(r) < 0$. The integration in eq 16 was done from $Q_{MIN} = 0.1$ Å^{-1} to $Q_{MAX} = 0.5$ Å^{-1}; the integral from 0 to Q_{MIN} was evaluated using eq 12 and the $I_{EXP}(0)$ and $R^2_{g(EXP)}$ values. D_{THEO} was found from $\gamma_{THEO}(r)$ under the assumption that $\gamma_{THEO}(D_{THEO}) \equiv 0$.

We did not use Porod's law in the data analysis, because the scattering by molecules as small as cyclodextrins is far from reaching the asymptotic regime "$I(Q) = const_1/Q^4 + const_2$" for $Q < 0.5$ Å^{-1}; this was confirmed by tests on $I_{THEO/SAXS}(Q)$ for CDs and mCDs. We did not transform experimental scattering curves to real space to get $\gamma_{EXP}(r)$ because $\gamma_{EXP}(r)$ is the Fourier transform of I(Q) (eq 8), and consequently it contains exactly the same information as I(Q). Moreover, because of our limited Q range, $\gamma_{EXP}(r)$ would not reveal the eventual existence of aggregates with a radius greater than $\approx\pi/0.05$ Å$^{-1} \approx 60$ Å; that is, only oligomers would be seen. We also preferred an evaluation of D_{THEO} through F(r) rather than through $\gamma_{EXP}(r)$ obtained by general powerful procedures (as in ref 27), because the former way does not require any preliminary D estimate and is simpler.

3.2. Nondilute Solution Scattering. The scattering from a solution with concentration c, I(Q,c), is

$$I(Q,c) = S(Q,c) \times I(Q) \quad (17)$$

where S(Q,c) is the intermolecular structure factor. Equation 17 holds under the condition: $\langle|F(\boldsymbol{Q}) - f(\boldsymbol{Q})|^2\rangle_\Omega \approx \langle|F(\boldsymbol{Q}) - f(\boldsymbol{Q})|\rangle_\Omega^2$; for CDs and mCDs, the calculations done under homogeneous approximation show that it holds for $Q < 0.4$ Å^{-1}. The $S(Q = 0,c)$ value is related to the osmotic pressure of the solution, Π:

$$S(0,c) = (RT/M) \times (\partial\Pi/\partial c)^{-1} \quad (18)$$

Π can be expanded as a power series of the solute concentration:

$$\Pi/cRT = 1/M + A_2c + A_3c^2 + ... \quad (19)$$

where A_2 and A_3 are the second and the third virial coefficients, respectively. The equation that we fitted to S(0,c) data follows from eqs 18 and 19:

$$\{1/S(0,c) - 1\}/(Mc) = 2A_2 + 3A_3c \quad (20)$$

With Φ being the molar osmotic coefficient, eq 19 may be written as

$$\Pi = \Phi cRT \quad (21)$$

In infinitely dilute solutions, solute−solute interactions disappear, and the virial coefficients are all zero, $\Phi = 1$, and S(0,c) $= 1$. In real solutions, if these interactions are repulsive, $A_2 >$

0, and $\Phi > 1$, $S(0,c) < 1$; if they are attractive, $A_2 < 0$, $\Phi < 1$, and $S(0,c) > 1$.

We assume that in aqueous solution the structures of CDs and mCDs do not change appreciably with either temperature or concentration. Thus, any variation in $I(Q,c)$ curves, if no oligomers or aggregates are formed, is solely due to changes in the solute−solute interactions and, consequently, in $S(Q,c)$. Generally, repulsive solute−solute interactions manifest themselves in SAXS and SANS spectra through a decrease (and attractive interactions through an increase) of scattering intensity at low Q values.

4. Results and Discussion

We recorded SAXS spectra of solutions in D_2O (instead of H_2O) to be able to compare the obtained results with those from our SANS measurements (in D_2O) and to apply the gathered information for the analysis of QENS spectra that were recorded for D_2O solutions as well.[9] At the beginning of the SAXS measurements, we recorded a sequence of scattering patterns from solutions of β-CD, γ-CD, and DIMEB and found no indication of sample damage due to the very intense synchrotron radiation. A solution of TRIMEG was irradiated for 1 h, and the subsequently recorded spectrum showed also no signs of radiation damage.

We assumed that the SAXS and SANS curves for the lowest solute concentrations (6.0, 9.3, 6.6, and 10.0 mg/mL {from 4.9 to 7.1 mM} for β-CD, γ-CD, DIMEB, and TRIMEG, respectively) represented, given that there were no oligomers or aggregates, the scattering from single solute molecules; that is, $I_{EXP}(Q,c) = I_{EXP}(Q)$. This assumption allowed us (i) to obtain the $R^2_{g(EXP)}$ and D_{EXP} values, (ii) to compare the theoretical scattering curves, $I_{THEO}(Q)$, with the experimental ones, and (iii) to evaluate intermolecular structure factors and virial coefficients.

4.1. SAXS from Dilute Solutions: $Q \rightarrow 0$ and Excluded Volume. The matching of the calculated and experimental scattering curves in the low Q region allows us to determine an *EX* value and, consequently, the excluded volume (V) of the molecule, $V = V_{THEO}(EX)$ (see section 3.1). We will compare the so obtained volumes to the apparent molar volumes at infinite dilution (V^0). Note that the latter are obtained under the assumption that the change of the water structure near the surface of the solute can be neglected.

At 25 °C, the (literature) V^0 values determined from density measurements of aqueous solutions are 711 and 803 [cm^3/mol] for β-CD[28] and γ-CD,[29] respectively. Per molecule, these values are 1181 and 1333 Å^3, and higher than the V_{THEO} values evaluated with $EX = 0$ (1003 and 1195 Å^3). For γ-CD, we took $EX = 0.1$ Å (which yields $V_{THEO} = 1302$ Å^3) and chose f_{H2O} within the uncertainty of the ratio $I_{H2O}/I_{E.C.}$ (see eq 2) such as to match $I_{EXP/SAXS}(Q)$ to $I_{THEO/SAXS}(Q)$ at low Q values. The so obtained f_{H2O} value was further used to get *EX* values for β-CD, DIMEB, and TRIMEG. The final *EX* and V_{THEO} values are in Table 1.

For β-CD, the agreement of V_{THEO} with V^0 is good: $EX = 0.23$ Å yields $V_{THEO} = 1200$ Å^3. We can not check which *EX* values would result in a good agreement between V_{THEO} and V^0 for DIMEB and TRIMEG because we did not measure the densities of their aqueous solutions. For comparison, the reported[28] V^0 value for per-trimethylated-β-CD is 1077 [cm^3/mol] or 1788 Å^3, while our computations using its crystal structure[5] yielded $V_{THEO} = 1779$ Å^3 at $EX = 0.26$ Å.

Qualitatively, *EX* increases the excluded volume by adding a shell of thickness *EX* Å around the vdW volume. That such a shell is required appears to be reasonable, because in eqs 6−9, the integration is performed over the volume excluded by the molecule in solution, not over the vdW volume of the molecule. For example, Shahidi et al.[28] used such a shell (with $EX = 0.57$ Å) when modeling partial molar volumes of cyclic ethers.

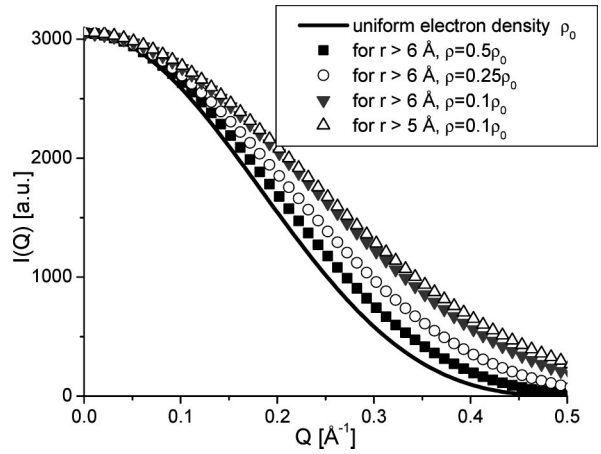

Figure 4. Scattering curves calculated for a sphere of radius 9 Å and normalized to the square of the average electron density. Nonhomogeneous electron density distribution is modeled by the inner core (with electron density ρ_0) and outer shell with $\rho < \rho_0$.

The here determined *EX* values may be, at least partially, explained by considering the structure of the solutes. mCDs are by far more conformationally flexible than native CDs because the O(2)−CH_3 and O(3)−CH_3 groups can rotate about the C(2)−O(2) and C(3)−O(3) bonds, and the O(6)−CH_3 groups are even more variable in their conformations, because they can rotate about C(5)−C(6)−O(6) bonds. This may be one of the reasons why *EX* values for DIMEB and TRIMEG are higher than *EX* for γ-CD. Furthermore, native CDs are rigidly confined to "round", annular structures that are stabilized by O(2)−H···O(3) and O(2)···H−O(3) hydrogen bonds around the macrocycle (Figures 1 and 2); in DIMEB, only the O(2)···H−O(3) hydrogen bonds are possible, but they stabilize the structure as well. By contrast, in TRIMEG, the O(2)···H−O(3) hydrogen bonds can not form, rendering this macrocycle much more flexible, and two glucoses can even rotate by ∼180° (in anti-conformation) with respect to the other six glucoses that are in syn,[7] as shown in Figure 2. This may contribute to a higher *EX* for TRIMEG relative to DIMEB, but because *EX* for DIMEB is the same as for per-trimethylated-β-CD, there may be other reasons beyond structural flexibility. Such reasons may be solvent−solute interactions and hydration shell structure. Indeed, the *EX* value for β-CD is higher than that for γ-CD, and β-CD is much less soluble in water[3] than γ-CD because of ordering of water around the macrocycle.[30,31]

The *EX* value can be obtained more reliably (or even at all) for small molecules because the relative change of the scattering due to a change of the excluded volume is proportional to $(\partial I(Q)/\partial V)/I(Q)$ and, at $Q \rightarrow 0$, to $1/V$. That is, the greater the volume, the smaller the relative change of the scattering due to a nonzero *EX*. Most of molecules studied by SAXS or SANS are at least several times greater than CDs. Consequently, the neglect of a thin shell of the thickness *EX* Å would little worsen the agreement of the experimental and calculated data. Moreover, the complexity of big molecules (e.g., many possible conformations) leads to uncertainties in the excluded volumes that are probably even greater than the volume changes due to *EX* lying between 0 to 0.5 Å.

4.2. SAXS from Dilute Solutions: Q Dependence. The $I_{EXP/SAXS}(Q)$ and $I_{THEO/SAXS}(Q)$ curves for CDs and mCDs are shown

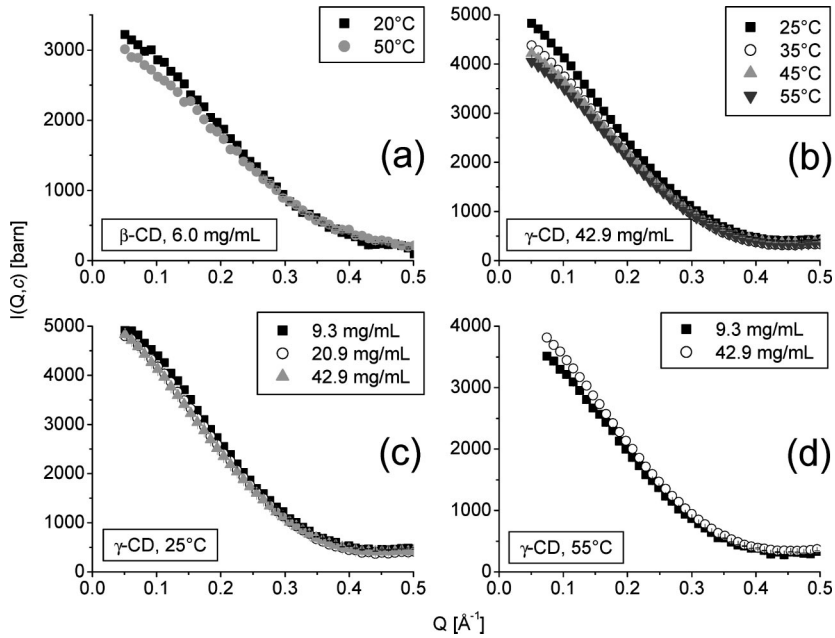

Figure 5. Temperature and concentration dependence of SAXS for β-CD (a) and γ-CD (b−d) dissolved in D_2O.

in Figure 3. For β- and γ-CD, the agreement is good for $Q < 0.4$ Å^{-1} (Figure 3a,b), indicating that in this Q range the homogeneous approximation is valid and $(\Delta\rho_{AV})^2I_0(Q)$ (see eq 10) constitutes most of the scattering. For mCDs, the agreement is poor (Figure 3c,d), indicating that the terms $\Delta\rho_{AV}I_{01}(Q)$ and $I_1(Q)$ contribute substantially to the scattering curve. The reason for this is the presence of methyl groups, which results in (i) a decrease (compared with β- and γ-CD; see Table 1) of the contrast and thus the scattering term $(\Delta\rho_{AV})^2I_0(Q)$ and (ii) a greater variation of the electron density over the volume of the molecule. Indeed, OH and CH_3 groups have equal number of electrons, but, as seen already from their vdW volumes (8.04 and 13.67 cm^3/mol, respectively[32]), they contribute differently to the molecule's excluded volume. In addition, *EX* values are greater for mCDs (Table 1), thus, resulting in a further increase of the mCDs' excluded volumes. Considering the above, an mCD molecule is qualitatively like a sphere with the outer shell having substantially lower electron density than the core. The exact calculations for scattering by such a sphere (Figure 4) illustrate the origin of the discrepancy between the calculated and the experimental curves in Figure 3c,d. We stress that scattering due to inhomogeneities (terms $\Delta\rho_{AV}I_{01}(Q) + I_1(Q)$ in eq 10) could not be subtracted from the experimental curve. The common method to do such a subtraction (see, e.g., p 1745 in ref 17) makes use of Porod's law, but we could not apply it here; see section 3.1.

$R^2_{g(EXP)}$ derived from the curves in Figure 3 using eq 12 are in good agreement with $R^2_{g(THEO)}$ for β- and γ-CD but not for DIMEB and TRIMEG (Table 1). The discrepancy observed for mCDs can be explained by the dependence of $R^2_{g(EXP)}$ on the scattering contrast; see eq 13. We neglect the term $\beta/(\Delta\rho_{AV})^2$ because for molecules with an axial symmetry (like CDs and mCDs), β (eq 15) is small. α evaluated from eq 14 is negative because the electron density is lower at the periphery because of the hydrogen atoms of the methyl groups. Since for X-ray scattering from solutions of mCDs in D_2O $\Delta\rho_{AV}$ values are positive (Table 1), the R^2_g predicted by eq 13 for DIMEB and TRIMEG are lower than the $R^2_{g(THEO)}$ and so are the observed $R^2_{g(EXP)}$. That the deviations of $R^2_{g(EXP)}$ and $I_{EXP/SAXS}(Q)$ from $R^2_{g(THEO)}$ and $I_{THEO/SAXS}(Q)$ are greater for TRIMEG than for DIMEB (Figure 3c,d and Table 1) indicates greater inhomogeneities in the electron density of TRIMEG. This is understandable, because TRIMEG has more methyl groups, and is more flexible than DIMEB (see section 4.1).

The agreement between D_{EXP} and D_{THEO} is good for β-CD, γ-CD, and DIMEB, but poor for TRIMEG (Table 1). We can not explain the poor agreement for TRIMEG, but the method we used to estimate D_{EXP} may give wrong results when scattering contribution from inhomogeneities in the electron density is significant.

Neither CDs nor mCDs formed oligomers, for if they did, a steeper increase of the scattering intensity toward the low Q region would have been observed (relative to the theoretical curve). If there were appreciable concentration of aggregates, this would lead, effectively, to a decrease of the concentration of the solute monomers. Such a decrease would result in an $I_{EXP/SAXS}(Q)$ curve lying lower than the $I_{THEO/SAXS}(Q)$ curve for high (>0.4 Å^{-1}) Q values, and this is definitely not the case (Figure 3). Thus, our results indicate that β-CD, γ-CD, DIMEB, and TRIMEG occur as monomers in aqueous solutions under the chosen conditions. This is also supported by osmotic pressure measurements; see section 4.5. By contrast, a light scattering (LS) study[33] claimed the presence of aggregates in α-, β-, and γ-CD dissolved in H_2O. A later LS study[34] found aggregates for β-CD (at 1.3 mg/mL in H_2O) and no aggregates or oligomers in H_2O solutions of α-CD, γ-CD, and DIMEB (they could not, however, determine the molecular mass of β-CD in the same manner as was done for the other studied CDs[34]).

4.3. Variation of SAXS Curves with Increasing Temperature and Solute Concentration. The β-CD scattering curve for $c = 6.0$ mg/mL is less steep for higher temperatures (Figure 5a), indicating (by a relative decrease of intensity toward $Q = 0$) that solute−solute interactions become more repulsive. Owing to the low solubility of β-CD in H_2O[3] (and even lower in D_2O), we could not measure β-CD solutions of higher concentrations, and consequently, we can not describe concentration-dependent experiments. For γ-CD, the SAXS temperature dependence shown in Figure 5b is similar as that for β-CD, in accord with a positive temperature coefficient of solubility of β- and γ-CD in water. Figure 5c,d shows the concentration dependence of $I_{EXP/SAXS}(Q)$ for γ-CD at 25 and 55 °C. While at 25 °C, the intensity slightly decreases at low Q upon increase of concentra-

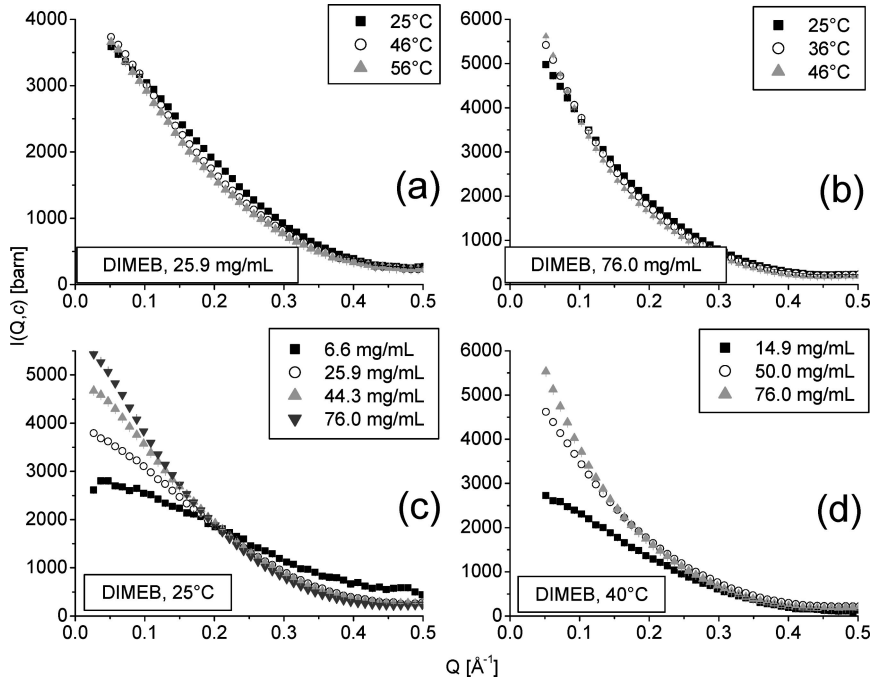

Figure 6. Temperature and concentration dependence of SAXS for DIMEB dissolved in D_2O.

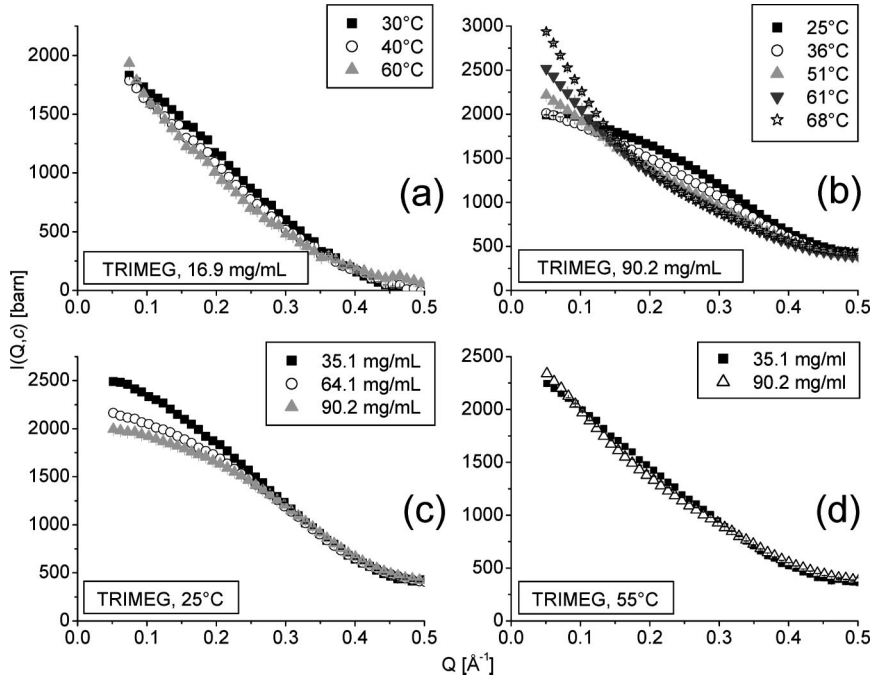

Figure 7. Temperature and concentration dependence of SAXS for TRIMEG dissolved in D_2O.

tion (indicating more repulsive interactions); the opposite is true at 55 °C. This probably reflects the change in the balance between the hard core repulsive interactions and the attractive (hydrophobic or vdW) interactions; see also section 4.6.

Higher temperature leads to an increase of attractive interactions in solutions of DIMEB; this is reflected in the shape of the SAXS curve, which becomes more concave (due to the greater intensity at low Q; Figure 6a,b). An increase of DIMEB concentration changes the curves in a similar way at 25 and 40 °C, although more substantially, indicating that attractive solute−solute interactions become stronger (Figure 6c,d).

For TRIMEG, as for DIMEB, the SAXS curve changes from convex at room temperature to increasingly more concave with increasing temperature (Figure 7a,b), indicating stronger attractive interactions. As for concentration dependence at 25 °C (Figure 7c), a decrease in the intensity at low Q when the TRIMEG concentration increases means that the net interactions become more repulsive. At 55 °C (Figure 7d), at higher solute concentrations, attractive interactions dominate over hard core repulsion; consequently, $I_{EXP/SAXS}(Q,c)$ becomes larger at low Q, similar to the change in DIMEB scattering curves with increasing concentration; see Figure 6c,d.

Thus, an increase in concentration leads to an increase in attractive interactions both at 25 °C and at 40 °C for DIMEB (Figure 6c,d); but for TRIMEG, it leads to an increase in the net repulsive interactions at 25 °C (Figure 7c) and to net attractive interactions at 55 °C (Figure 7d). Such contrast is in accord with the solubility of the two mCDs: at a concentration

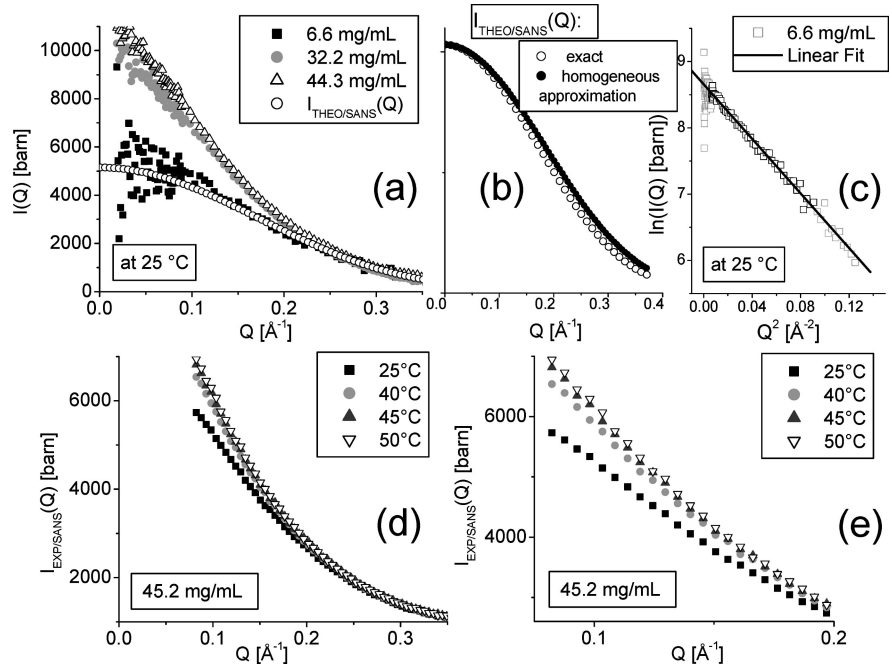

Figure 8. SANS results for D_2O solutions of DIMEB. (a) Experimental and theoretical ($I_{THEO/SANS}(Q)$) SANS curves. (b) $I_{THEO/SANS}(Q)$ curves calculated exactly (same as in a), and under the homogeneous approximation. (c) Guinier plot for $I_{EXP/SANS}(Q,c) = 6.6$ mg/mL (open squares); the fitted range is marked by black open squares, gray open squares were masked (to cut the high Q region and to exclude noisy data in the low Q region). (d) Temperature dependence of the $I_{EXP/SANS}(Q,c)$ curve. (e) Same as in d, magnified.

of 44.3 mg/mL{33.3 mM} in D_2O, DIMEB crystallizes at about 50 °C, whereas at 64.1 mg/mL{39.3 mM} in D_2O, TRIMEG crystallizes at >70 °C.

(In Figure 7d the SAXS curve for $c = 35.1$ mg/mL is upshifted by an additive constant so that both SAXS curves coincide at high Q values. The reasons for an eventual shift of SAXS curves relative to each other, as well as the values of the additive constants are discussed in Appendix (Supporting Information)).

4.4. SANS Results. The evaluation of the theoretical SANS curve, $I_{THEO/SANS}(Q)$, did not rely on the homogeneous approximation, as was the case for $I_{THEO/SAXS}(Q)$. Therefore, $I_{THEO/SANS}(Q)$ must agree with $I_{EXP/SANS}(Q,c)$ for low concentrations. Indeed, Figure 8a shows that the theoretical curve for DIMEB is similar to the experimental one for $c = 6.6$ mg/mL, and that the $I_{EXP/SANS}(Q,c)$ curves change with increasing concentration in the same fashion as shown by SAXS curves in Figure 6c. To record spectra for $Q < 0.1$ Å^{-1} in Figure 8a, we increased the sample-to-detector distance four times but left counting times unchanged, and this explains the wider scatter of data points in the low Q region. (The value of I_{INC} in eq 3 was increased so that all $I_{EXP/SANS}(Q,c)$ curves overlap approximately at $Q \approx 0.35$ Å^{-1} in Figure 8a. This "shift" accounts for the sample-dependent background caused by the contamination of D_2O with even a small amount of H_2O and is justified in view of the SAXS results for DIMEB; see Figure 6c).

As shown in Table 1, the absolute scattering contrast for DIMEB dissolved in D_2O is larger for neutron than it is for X-ray scattering. Therefore, for SANS relative to SAXS, the scattering contribution $(\Delta\rho_{AV})^2 I_0(Q)$ constitutes a greater part of the total scattering curve, and the homogeneous approximation is justified to a greater extent. Figure 8b confirms this: the $I_{THEO/SANS}(Q)$ curve evaluated using the homogeneous approximation is only slightly above $I_{THEO/SANS}(Q)$ calculated exactly.

$R^2_{g(EXP)}$ evaluated from $I_{EXP/SANS}(Q,c)$ for DIMEB at $c = 6.6$ mg/mL (Figure 8c) is 61.7 Å^2 and larger than the $R^2_{g(THEO)}$ value which is 45.2 Å^2; see Table 1. This difference is in a qualitative agreement with eq 13 (i) because the scattering contrast is negative and (ii) because hydrogen has a negative neutron coherent scattering length, and there are many hydrogen atoms at the periphery of DIMEB; the scattering length density is lower at the periphery of DIMEB, rendering α in eq 14 negative. D_{EXP} from SANS is ≈40% greater than D_{THEO} (Table 1), which we explain by the sensitivity of the D_{EXP} determination procedure for the correction for the incoherent scattering background. While the relative significance of this background decreases with the size of the molecule, it is high for small molecules such as CDs or mCDs.

The $I_{EXP/SANS}(Q,c)$ curves of DIMEB for different temperatures are shown in Figure 8d,e (I_{INC} was not subtracted here). The trend is the same as found by SAXS: upon increase of temperature, the intensity rises in the low Q region and the curve becomes more concave.

4.5. Comparison with Osmotic Pressure Measurements. For γ-CD at 25 °C, the reported[29] osmotic coefficients (Φ) decrease steadily with increasing solute concentration, thus, indicating a slight increase in attractive solute−solute interactions (see eq 21 and below). This is in agreement with our observations at 55 °C (Figure 5d) but not at 25 °C (Figure 5c), where the change in the scattering at low Q, although small, indicates repulsive solute−solute interactions. For the highest concentration studied here, $c = 42.9$ mg/mL {33.1 mM}, the extrapolated Φ value from the literature[29] is ≈0.98. Clearly, the net solute−solute interactions are weak, and the conclusion on "attractive versus repulsive" is uncertain, because it is based on scattering for $Q > 0.05$ Å^{-1}.

Osmotic coefficients reported for DIMEB[35] are substantially smaller than unity ($\Phi < 0.9$ for $c > 26.6$ mg/mL {20 mM} at 25 °C) and decrease markedly both upon increase of temperature and concentration. This is in agreement with an increase of attractive interactions as demonstrated by our SAXS and SANS data. For several DIMEB concentrations, the difference in the Φ values observed for 25 ° and 35 °C is higher than the

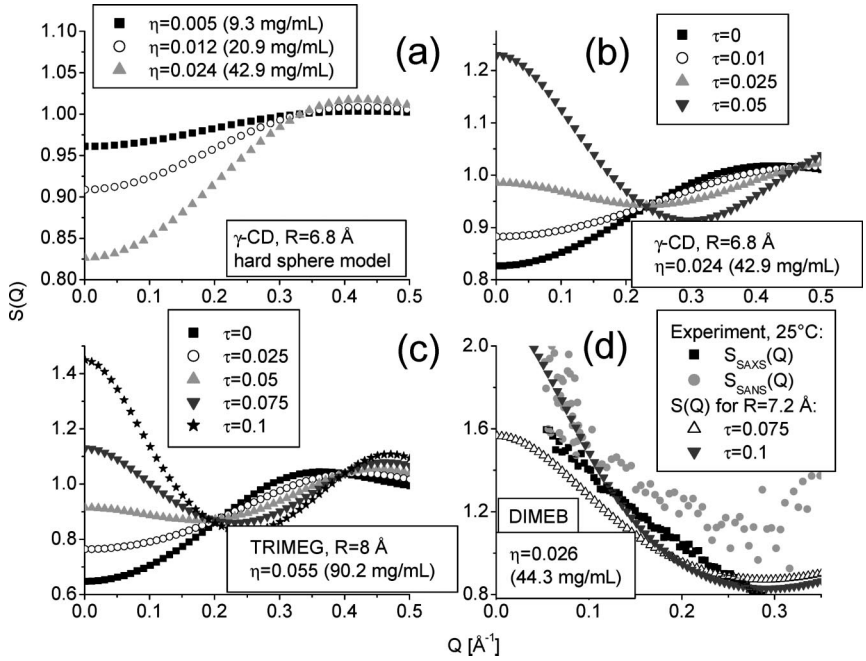

Figure 9. Theoretical (for γ-CD, TRIMEG, DIMEB) and experimental (for DIMEB only, in d) intermolecular structure factors, S(Q). (a) Structure factors for hard sphere model; R is the radius of the sphere; η is the solute volume fraction. (b−d) Structure factors for the sticky hard sphere model,[10] τ is "stickiness" (the greater the τ, the greater the attraction between the spheres). See section 4.6.

difference in the Φ values observed at 35 and 45 °C.[35] This agrees with data shown for SAXS (Figure 6a,b) and for SANS (Figure 8e).

Note, that if there were aggregates in solutions of CDs and mCDs, the corresponding osmotic coefficients would be much smaller than unity, because the osmotic pressure depends on the concentration of solute particles irrespective of their type.

4.6. S(Q) Analysis. Using SAXS curves at 25 °C for mCDs, we calculated S(Q,c) from eq 17 as follows: $S(Q,c) = I_{EXP/SAXS}(Q,c)/I_{EXP/SAXS}(Q,c_{min})$, where c_{min} is 6.6 and 10 mg/mL for DIMEB and TRIMEG, respectively. (Concentration effects for $c = c_{min}$ were neglected. As shown in section 4.2, only monomeric forms of mCDs are present in solution at these concentrations). S(0,c) values for the three highest concentrations were found by extrapolation of S(Q,c) to $Q = 0$ and fitted to eq 20.

For DIMEB, the fit yielded $A_2 = -5.2 \times 10^{-3} \pm 3 \times 10^{-5}$ [mol mL g^{-2}] and $A_3 = 2.45 \times 10^{-2} \pm 4 \times 10^{-4}$ [mol mL^2 g^{-3}]. Another study[34] found for DIMEB dissolved in H_2O, $A_2 \approx -2.5 \times 10^{-3}$ [mol mL g^{-2}] at 25 °C, the difference being possibly due to the neglect of A_3 in ref 34. If we neglect A_3, A_2 values are -4.2×10^{-3}, -3.6×10^{-3}, and -2.4×10^{-3} [mol mL g^{-2}] for $c = 25.9$, 44.3, and 76.0 mg/mL, respectively. For TRIMEG, the linear fit to eq 20 (i.e., setting $A_3 = 0$) was poor, indicating error(s) in S(0,c) data. Such errors are more likely to occur for TRIMEG because (i) for a higher c_{min}, S(Q,c) is more biased, and (ii) the greater the S(0,c) value is, the smaller will be the error in the $\{1/S(0,c) - 1\}$ value.

To consider the contributions from attractive and repulsive solute−solute interactions, we represented CDs and mCDs by spheres with radii chosen so that the volumes of these spheres matched the V_{THEO} values in Table 1. Figure 9a shows the intermolecular structure factor, S(Q), calculated within the Percus−Yevick approximation for the hard sphere model (see, e.g., ref 36) for γ-CD at the concentrations studied here. Clearly, if there were only hard sphere (HS) interactions, the scattering curves in Figure 5c,d would substantially decrease toward low Q region with increasing concentration, and the osmotic coefficients would be higher than unity. Therefore, there are attractive interactions that partially compensate for the repulsive HS interactions, but they are not electrostatic because CDs and mCDs are uncharged molecules at neutral pH ($pK_a \approx 12$ for γ-CD at 25 °C[37]). To account for these attractive interactions, we used the model of sticky hard spheres,[10,36] where the dimensionless parameter τ ($\tau > 0$) controls the strength of attractive interactions; if $\tau = 0$, S(Q) for the HS model is obtained. The influence of τ values on S(Q) curves for a γ-CD solution with concentration 42.9 mg/mL is shown in Figure 9b, and this influence (for τ values between 0.01 to 0.025) explains the weak concentration dependence of I(Q,c) curves in Figure 5c,d.

For TRIMEG, the modeled S(Q) curves for a concentration of 90.2 mg/mL and various τ values are shown in Figure 9c. The decrease in S(Q) toward low Q region for $\tau < 0.05$ corresponds to the concentration dependence of SAXS curves shown in Figure 7c and is valid when the repulsive HS interactions dominate over attractive interactions. The S(Q) curves for $\tau > 0.075$ correspond to the SAXS concentration dependence in Figure 7d, the case when attraction dominates over HS repulsion.

For DIMEB, the experimental S(Q) curves evaluated from the SAXS and SANS curves for $c = 44.3$ mg/mL (see above) are shown in Figure 9d. By considering the scatter of the SANS data points and an uncertainty in the I_{INC} value, neutron and X-ray scattering give similar results, and the calculated S(Q) curves qualitatively reproduce the experimental ones.

Before any quantitative comparison between the experimental and the theoretical S(Q) curves can be made, more precise S(Q) determinations are required. In addition, the temperature dependence of the scattering by dilute solutions of mCDs must be studied to verify the assumption that any changes of scattering curve with temperature is due to S(Q,c) only. For CDs, such verification is less important because they are more rigid (section 4.1).

4.7. SANS versus SAXS. The advantage of SANS is that, if the crystal structure of a given molecule is available, the

scattering curve calculated without any approximations can be compared to the measured one. The SAXS curve can only be calculated in the homogeneous approximation that is valid within a limited Q region, and it is not always known how broad this region is. Thus, for investigation of single molecule structure and solute−solvent interactions (through the *EX* parameter), SANS is better than SAXS, if measurements with sufficient counting times may be done. But, SANS spectra from solutions of small molecules like CDs have a significant incoherent background, which is especially difficult to correct for when concentrations are low.

For studies of solute−solute interactions as a function of temperature, concentration, and so forth, SAXS is better suited (if there is no radiation damage) because the measurements take less time. In such studies, modeling of single molecule scattering is not necessary, and the accuracy of the SAXS curves for the low solute concentrations does not suffer from the incoherent scattering background.

5. Conclusions

We describe here the first SAXS and SANS measurements on β- and γ-CD and their methylated derivatives, DIMEB and TRIMEG, and show the feasibility of such a study (which is not self-evident considering the small molecular masses (1−1.6 kDa) of the studied compounds).

For CDs, the experimental SAXS curves ($I_{EXP/SAXS}(Q,c)$) and the squares of gyration radii ($R^2_{g(EXP)}$) agreed with the ones calculated from the crystal structures under the assumption of uniform distribution of electron density. This was not so for mCDs, apparently because inhomogeneities in electron density due to the appended methyl groups contribute substantially to $I_{EXP/SAXS}(Q,c)$, and consequently to the $R^2_{g(EXP)}$ values. An evidence for this can be seen in the greater discrepancies found for TRIMEG compared with DIMEB, which is in agreement with the fact that the former has more methyl groups (and thus a greater extent of inhomogeneities) than the latter. Transformation of $I_{EXP/SAXS}(Q,c)$ to an absolute scale confirmed that the studied compounds existed only as monomers under the chosen conditions. This also showed that the solute excluded volumes are greater than van der Waals volumes, due to, effectively, the presence of a thin shell with a thickness between 0.1 Å and 0.33 Å. The differences in the shell's thickness were related to the solute's structure and to solute−water interactions. By contrast to SAXS, a good agreement was found between the calculated (without any assumptions) and the experimental SANS curves for dilute solutions of DIMEB.

We studied the influence of temperature and concentration on SAXS and (for DIMEB only) on SANS; the results agree with osmotic pressure measurements. The scattering curves for β- and γ-CD indicated an increase of repulsive solute−solute interactions with increasing temperature (Figure 5a,b), in accord with their positive solubility coefficient in water. For DIMEB, attractive intermolecular interactions have been observed in all SAXS (Figure 6) and SANS (Figure 8d,e) curves. On the contrary, while TRIMEG solutions showed net repulsive interactions at room temperature, the interactions became increasingly more attractive when the temperature was increased (SAXS, Figure 7). This agrees with the fact that TRIMEG crystallizes at significantly (more than 20 °C) higher temperature than DIMEB. Finally, the variation of the scattering curves with temperature and concentration was qualitatively explained by a sticky hard sphere model.

Acknowledgment. We thank P. V. Konarev and D. I. Svergun for valuable assistance during the X33 experiment that was supported through the European Community−Research Infrastructure Action under the FP6 "Structuring the European Research Area Programme", Contract No. RII3-CT-2004-506008. One of the authors (A.K.) was supported by DFG Graduate College 788, Freie Universität Berlin. Two of us (A.K. and R.E.L.) thank the Hahn-Meitner-Institut for hospitality. We thank the referees for their constructive criticism which helped to improve the manuscript.

Supporting Information Available: Appendix with discussion of an eventual shift of SAXS curves by an additive constant. This material is available free of charge via the Internet at http://pubs.acs.org.

References and Notes

(1) Saenger, W.; Jacob, J.; Gessler, K.; Steiner, T.; Hoffmann, D.; Sanbe, H.; Koizumi, K.; Smith, S. M.; Takaha, T. *Chem. Rev.* **1998**, *98*, 1787–1802.

(2) Uekama, K.; Irie, T. In *Cyclodextrins and their industrial Uses*; Duchêne, D. Ed.; Editions de Santé: Paris, 1987; pp 395−439.

(3) Jozwiakowski, M. J.; Connors, K. A. *Carbohydr. Res.* **1985**, *143*, 51–59.

(4) Steiner, T.; Saenger, W. *Carbohyd. Res.* **1995**, *275*, 73–82.

(5) Steiner, T.; Saenger, W. *Angew. Chem., Int. Ed.* **1998**, *37*, 3404–3407.

(6) Aree, T.; Hoier, H.; Schulz, B.; Reck, G.; Saenger, W. *Angew. Chem., Int. Ed.* **2000**, *39*, 897–899.

(7) Aree, T.; Hoier, H.; Schulz, B.; Reck, G.; Saenger, W. *Carbohydr. Res.* **2000**, *328*, 399–407.

(8) Starikov, E. B.; Bräsicke, K.; Knapp, E. W.; Saenger, W. *Chem. Phys. Lett.* **2001**, *336*, 504–510.

(9) Kusmin, A.; Lechner, R. E.; Saenger, W. In *Quasi-Elastic Neutron Scattering Conference 2006 (QENS2006)*; Sokol, P. E., Kaiser, H., Baxter, D., Pynn, R., Bossev, D., Leuschner, M., Eds.;Mater. Res. Soc., Warrendale, PA, 2007; pp 37−44.

(10) Baxter, R. J. *J. Chem. Phys.* **1968**, *49*, 2770–2774.

(11) Boulin, C. J.; Kempf, R.; Gabriel, A.; Koch, M. H. J. *Nucl. Instrum. Meth. A* **1988**, *269*, 312–320.

(12) Konarev, P. V.; Volkov, V. V.; Sokolova, A. V.; Koch, M. H. J.; Svergun, D. I. *J. Appl. Crystallogr.* **2003**, *36*, 1277–1282.

(13) Orthaber, D.; Bergmann, A.; Glatter, O. *J. Appl. Crystallogr.* **2000**, *33*, 218–225.

(14) Keiderling, U.; Wiedenmann, A. *Physica B* **1995**, *213−214*, 895–897.

(15) Strunz, P.; Saroun, J.; Keiderling, U.; Wiedenmann, A.; Przenioslo, R. *J. Appl. Crystallogr.* **2000**, *33*, 829–833.

(16) Keiderling, U. *Appl. Phys. A: Mater. Sci. Process.* **2002**, *74*, s1455–s1457.

(17) Svergun, D. I.; Koch, M. H. J. *Rep. Prog. Phys.* **2003**, *66*, 1735–1782.

(18) Koch, M. H. J.; Vachette, P.; Svergun, D. I. *Q. Rev. Biophys.* **2003**, *36*, 147–227.

(19) Fedorov, B. A.; Ptitsyn, O. B.; Voronin, L. A. *J. Appl. Crystallogr.* **1974**, *7*, 181–186.

(20) Müller, J. J. *J. Appl. Crystallogr.* **1983**, *16*, 74–82.

(21) Stuhrmann, H. B.; Miller, A. *J. Appl. Crystallogr.* **1978**, *11*, 325–345.

(22) Aree, T.; Schulz, B.; Reck, G. *J. Inclusion Phenom. Macrocyclic Chem.* **2003**, *47*, 39–45.

(23) Ding, J.; Steiner, T.; Zabel, V.; Hingerty, B. E.; Mason, S. A.; Saenger, W. *J. Am. Chem. Soc.* **1991**, *113*, 8081–8089.

(24) Aree, T.; Saenger, W.; Leibnitz, P.; Hoier, H. *Carbohydr. Res.* **1999**, *315*, 199–205.

(25) Rowland, R. S.; Taylor, R. *J. Phys. Chem.* **1996**, *100*, 7384–7391.

(26) Müller, J. J.; Schmidt, P. W.; Damaschun, G. *J. Appl. Crystallogr.* **1980**, *13*, 280–283.

(27) Glatter, O. *J. Appl. Crystallogr.* **1977**, *10*, 415–421.

(28) Shahidi, F.; Farrell, P. G.; Edward, J. T. *J. Solution Chem.* **1976**, *5*, 807–816.

(29) Miyajima, K.; Sawada, M.; Nakagaki, M. *Bull. Chem. Soc. Jpn.* **1983**, *56*, 3556–3560.

(30) Linert, W.; Margl, P.; Renz, F. *Chem. Phys.* **1992**, *161*, 327–338.

(31) Naidoo, K. J.; Chen, J. Y.-J.; Jansson, J. L. M.; Widmalm, G.; Maliniak, A. *J. Phys. Chem. B* **2004**, *108*, 4236–4238.
(32) Bondi, A. *J. Phys. Chem.* **1964**, *68*, 441–451.
(33) Coleman, A. W.; Nicolis, I.; Keller, N.; Dalbiez, J. P. *J. Incl. Phenomen. Mol. Recogn.* **1992**, *13*, 139–143.
(34) Gaitano, G. G.; Brown, W.; Tardajos, G. J. *J. Phys. Chem. B* **1997**, *101*, 710–719.
(35) Miyajima, K.; Mukai, T.; Nakagaki, M.; Otagiri, M.; Uekama, K. *Bull. Chem. Soc. Jpn.* **1986**, *59*, 643–644.
(36) Pedersen, J. S. *Adv. Colloid Interface Sci.* **1997**, *70*, 171–210.
(37) Gelb, R. I.; Schwartz, L. M.; Laufer, D. A. *Bioorg. Chem.* **1982**, *11*, 274–280.

JP802031W